

Constraining ultra slow roll inflation using cosmological datasets

H. V. Ragavendra^{1*}, Anjan Kumar Sarkar^{2†} and Shiv K. Sethi^{1‡}

¹Raman Research Institute, C. V. Raman Avenue, Sadashivanagar, Bengaluru 560080, India

²National Centre for Radio Astrophysics, TIFR, Pune University Campus, Post Bag 3, Pune 411 007, India.

E-mail: *ragavendra@rrimail.ri.res.in, †asarkar@ncra.tifr.res.in, ‡sethi@rri.res.in

Abstract. In recent years, the detection of gravitational waves by LIGO and PTA collaborations have raised the intriguing possibility of excess matter power at small scales. Such an increase can be achieved by ultra slow roll (USR) phase during inflationary epoch. We constrain excess power over small scales within the framework of such models using cosmological datasets, particularly of CMB anisotropies and Lyman- α . We parameterize the USR phase in terms of the e-fold at the onset of USR (counted from the end of inflation) \bar{N}_1 and the duration of USR phase ΔN . The former dictates the scale of enhancement in the primordial power spectrum, while the latter determines the amplitude of such an enhancement. From a joint dataset of CMB and galaxy surveys, we obtain $\bar{N}_1 \lesssim 45$ with no bound on ΔN . This in turn implies that the scales over which the power spectrum can deviate significantly from the nearly scale invariant behavior of a typical slow-roll model is $k \gtrsim 1 \text{ Mpc}^{-1}$. On the other hand, the Lyman- α data is sensitive to baryonic power spectrum along the line of sight. We consider a semi-analytic theoretical method and high spectral-resolution Lyman- α data to constrain the model. The Lyman- α data limits both the USR parameters: $\bar{N}_1 \lesssim 41$ and $\Delta N \lesssim 0.4$. This constrains the amplitude of the power spectrum enhancement to be less than a factor of hundred over scales $1 \lesssim k/\text{Mpc}^{-1} \lesssim 100$, thereby considerably improving the constraint on power over these scales as compared to the bounds arrived at from CMB spectral distortion.

Contents

1	Introduction	1
2	Model of ultra-slow roll inflation	3
3	Results	6
3.1	CMB and galaxy survey data	6
3.1.1	Five parameter model	7
3.1.2	Two parameter model	10
3.2	Lyman- α forest	11
4	Conclusion	15

1 Introduction

The current cosmological data bears out the Λ CDM model at large scales ($k \lesssim 0.2 \text{ Mpc}^{-1}$). At smaller scales, the situation remains unsettled. While a set of observables suggest decrement of matter power at small scales, the enhancement of primordial scalar power at small scales is also a feature that has been sought after in the recent literature. Such enhancement leads to production of primordial black holes (PBHs) and secondary gravitational waves (GWs) and so models of primordial universe that effect such a feature have been constructed and examined extensively (see for reviews, Refs. [1–3]). This effort has been spurred by the detection of mergers of supermassive black-holes by LIGO and, recently, with the data release of PTA which claims the detection of stochastic GWs [4–8]. It has been suggested that the black-holes of the LIGO merger events are primordial black holes (see Refs. [9–14] and references therein). The data of PTA suggests that the scalar-induced secondary GWs seem to be the best-fit candidate to explain the signal [15–26].

Amongst the many models of early universe that may lead to the desired enhancement of scalar power over small scales, inflationary models with a brief epoch of ultra slow roll (USR) seem to be the ones that effectively achieve the required feature. Such models are realised by a variety of potentials with features such as (near-)inflection points, a break, a bump or a dip in them [27–44] (see also [45] for a brief review of such potentials). There are also attempts at reconstructing this model using the characteristic behavior of the first slow roll parameter [46–51]. USR models while amplifying the scalar power, also lead to certain tell-tale features in the spectrum. Their scalar power spectrum contains a unique dip in the amplitude just prior to the sharp rise in power [52, 53]¹. The rise is typically of shape k^4 until the peak amplitude is achieved [46, 55, 56]. The shape post the peak is determined by the dynamics of inflation after the phase of USR.

The crucial aspects in such a spectrum are the location of the peak and the amount of enhancement of power over the typical nearly scale-invariant amplitude over large scales. These features are determined by the onset and duration of the USR phase during inflation. In the context of production of PBHs and secondary GWs, the location of peak dictates the mass of PBHs and the frequency of the peak amplitude in the spectral density of GWs, denoted as Ω_{GW} . The amount of enhancement in turn determines the population of PBHs

¹This dip is at the tree-level power spectrum and may be modified or filled in by loop-level contributions [54].

and the amplitude of Ω_{GW} at its maximum. Thus the onset and duration of USR have a direct impact on the characteristics of the relevant observables.

Since the onset of USR dictates the relevant mass of PBHs or frequency of GWs, it is usually tuned to values as per the desired range. The duration of USR is also tuned to achieve the required population fraction of PBHs or the amplitude of GWs. The production of PBHs is exponentially sensitive to the peak amplitude of scalar power, and therefore on the duration of USR. Hence, these parameters are fine-tuned in models that attempt to achieve significant fraction of PBHs along with secondary GWs.

There have been attempts in the literature to examine the consistency of models leading to enhanced power over small scales and constraints from CMB anisotropies over large scales. In Refs. [46, 49, 53, 57–62], there are discussions about the value of scalar spectral index and tensor-to-scalar ratio arising from such models over large scales and how they are often in tension with the CMB data. It is also noted that there can be strong running of spectral index when the enhancement in power is achieved closer to CMB scales [53, 63]. Ref. [61] specifically focuses on a multi-field model of inflation and, using an analytical template of power spectrum, arrives at bounds on parameters of the two-field potential through a Markov-chain Monte-Carlo (MCMC) analysis against CMB dataset. However, there are no rigorous constraints on the models of USR through similar analysis. In this work, we attempt to constrain the dynamics of USR, particularly its onset and duration during inflation, using MCMC analysis against a variety of datasets over large scales.

Before the details of our analysis, we briefly summarize some of the key outcomes of the USR phase, based on the behavior of various inflationary potentials leading to USR. Over the course of about 70 e-folds of inflation, we need about four decades of CMB scales to have a nearly scale-invariant spectrum with reasonably small tensor-to-scalar ratio for agreement with Planck data. Hence we may expect just the initial 14–16 e-folds to have slow-roll dynamics during which these scales can evolve from sufficiently deep inside the Hubble radius and grow into the super-Hubble regime. This allows USR to occur anywhere in the last 55 e-folds of inflation. This essentially leaves a wide window of e-folds where USR can occur and last. On the other hand, a broad bound on the duration of USR comes from the limit on the enhancement of power spectrum $\mathcal{P}_s(k) < 1$. Since $\mathcal{P}_s(k) \propto \exp(6\Delta N)$ (ΔN denoting the duration in e-folds) during USR, this restricts the duration to be less than about three e-folds. Besides, if USR were to occur over an epoch that enhances power around scales of $k \sim 10^4 \text{ Mpc}^{-1}$, then the bound on $\mathcal{P}_s(k) < 10^{-5}$ from spectral distortions restricts USR to be less than 1.5 e-folds in this particular regime [64, 65]. Beyond these broad bounds, there are no strong constraints on the epoch of USR.

In this work, we attempt to directly constrain the epoch of the earliest onset of USR and its duration during inflation. To achieve this, we characterize the model of USR using a general parameterization of the first slow roll parameter over the entire course of inflation. This parameterization captures the essential features of USR models at the level of background and allows us to compute the dynamics of first-order perturbations. Moreover, it has explicit parameters that determine the onset of USR phase, its duration, and the smoothness of transition from SR to USR phase. We discuss the setup and details of this model in section 2. In section 3, we test our models against data on a range of scales, in particular the CMB and Lyman- α datasets. We first perform a comparison of model against the data of CMB anisotropies from Planck and BICEP/KECK missions. We then include the datasets of galaxy surveys from BOSS and DES missions, along with CMB to inspect the improvement in the constraints. We observe that CMB anisotropy data provide the essential bounds on the

parameters and they are mildly improved by the later additions. We discuss this part of data analysis in section 3.1. To test our theoretical model against small-scale data, we use the evolution of effective optical depth from high spectral-resolution Lyman- α data [66]. The details of this method and the results of statistical comparison are given in section 3.2. Lastly, we discuss the crucial takeaways and outlook of our work in section 4.

2 Model of ultra-slow roll inflation

There are several potentials in the literature that achieve a brief epoch of USR during inflation (for a review of USR, refer [45]). These models have a phase where the canonical scalar field (inflaton ϕ) undergoes a phase of exponential decrease in the velocity in terms of e-folds N . Such dynamics of inflaton field is best studied through the behavior of the first slow roll parameter ϵ_1 . This parameter is defined with respect to the Hubble parameter H as

$$\epsilon_1(N) = -\frac{1}{H^2} \frac{dH}{dt}, \quad (2.1)$$

where t is the cosmic time. Using Friedmann equations in this case of inflation driven by a single canonical scalar field, it can be expressed as

$$\epsilon_1(N) = \frac{1}{2H^2} \left(\frac{d\phi}{dt} \right)^2 = \frac{1}{2} \left(\frac{d\phi}{dN} \right)^2. \quad (2.2)$$

Hence the phase of USR is defined by the exponential decrease of ϵ_1 in terms of e-folds N , contrary to the SR phase where it evolves much slowly.

A parameterization of $\epsilon_1(N)$ that captures this behavior suitably is convenient to understand the dynamics and also the corresponding effect on perturbations. There have been attempts at reconstruction of a brief epoch of USR during inflation, through parameterization of $\epsilon_1(N)$ in the literature [47, 48, 50]. Such parametric models of $\epsilon_1(N)$ are sought to generalize the dynamics of USR, without restricting to any specific potentials. We work with one such parametric model where the form of $\epsilon_1(N)$ is given by [45, 49]

$$\epsilon_1(N) = \frac{\epsilon_{1_i} e^{\epsilon_{2_i} N}}{2} \left[1 - \tanh \left(\frac{N - N_1}{\delta N_1} \right) \right] + \frac{\epsilon_{1_f}}{2} \left[1 + \tanh \left(\frac{N - N_1}{\delta N_1} \right) \right] + e^{\frac{N - N_e}{\delta N_e}}. \quad (2.3)$$

In this parametrization, the onset of USR is determined by N_1 and the smoothness of transition between USR and SR phases is determined by δN_1 . The duration of USR phase is controlled by ΔN which enters the model through ϵ_{1_f} , as we set $\epsilon_{1_f} = \epsilon_{1_i} \exp(-6 \Delta N)$. The onset and duration of USR, N_1 and ΔN , are the two essential parameters that we shall be varying to observe the effects on the scalar power over small scales. Thus our parametric model gives us a direct handle on the USR dynamics through the parameters N_1 and ΔN . We set the value of smoothness to be $\delta N_1 = 0.31$. This choice of value corresponds to setting $\epsilon_2 \simeq -6$. This is the typical value achieved by ϵ_2 in USR models driven by various potentials (refer [45] for details). Variation of this parameter alters the value of ϵ_2 and in turn affects the steepness of rise in scalar power. We retain this parameter at its fixed value throughout our analysis.

The transition to USR phase is effected at N_1 by the terms containing hyperbolic tangents. The value of ϵ_1 drops from ϵ_{1_i} to ϵ_{1_f} during the USR phase. Once it settles to ϵ_{1_f} , the final phase of SR begins and it lasts until the last term starts playing a role. The end of

inflation is achieved by making ϵ_1 reach unity using the last term. We achieve 72 e-folds of inflation by setting $N_e = 72$ and the rapidity of the rise at the end is fixed as $\delta N_e = 0.55$.

The evolution of other background quantities such as the inflaton $\phi(N)$ and Hubble parameter $H(N)$ can be obtained from the behavior of $\epsilon_1(N)$ by inverting the relations (2.1) and (2.2) as

$$\phi(N) = \phi_i - \int_0^N dN' \sqrt{2\epsilon_1(N')} M_{\text{Pl}}, \quad (2.4)$$

$$H(N) = H_i \exp \left[- \int_0^N dN' \epsilon_1(N') \right], \quad (2.5)$$

along with suitable choice of initial conditions for respective quantities, namely the field value ϕ_i and the Hubble parameter H_i . The shape of the potential $V(\phi)$ can also be obtained from the behavior of $\phi(N)$ and $V(N) = [3 - \epsilon_1(N)] H^2(N) M_{\text{Pl}}^2$ ².

We numerically evolve the scalar and tensor perturbations over the background that is modelled through $\epsilon_1(N)$ and compute the corresponding spectra close to the end of inflation, well past the epoch of USR. The dimensionless power spectra of the scalar and tensor perturbations are defined, in terms of the associated mode functions f_k and g_k respectively, as [67–71]

$$\mathcal{P}_s(k) = \frac{k^3}{2\pi^2} |f_k|^2, \quad (2.6)$$

$$\mathcal{P}_T(k) = 4 \frac{k^3}{2\pi^2} |g_k|^2. \quad (2.7)$$

The pivot scale $k_p = 0.05 \text{ Mpc}^{-1}$ is set to exit the Hubble radius 50 e-folds before the end of inflation, i.e., at $N_p = 22$ in our parametrization. Thus the scales of CMB $k = [10^{-4}, 1] \text{ Mpc}^{-1}$ are set to exit the Hubble radius during $N = [16, 25]$ of our model. The choices of N_p , and $N_e = 72$ earlier, are made so as to let the largest observable scale (with $k \simeq 10^{-4} \text{ Mpc}^{-1}$) evolve from sufficiently deep inside the Hubble radius, for about 15 e-folds. This duration also dilutes imprints of any preceding non-inflationary epoch that could affect the evolution of perturbations. To relate to the convention of counting e-folds from the end of inflation, let us define

$$\bar{N} = N_e - N, \quad (2.8)$$

which in our case becomes $\bar{N} = 72 - N$. Thus, in terms of \bar{N} , the pivot scale exits Hubble radius at $\bar{N} = 50$ and the range corresponding to CMB scales is $\bar{N} = [56, 47]$. We shall use \bar{N} in later analysis, when we interpret various bounds on e-folds.

The behavior of scalar power spectrum for the range of parameters we work with is presented in Fig. 1. We observe that our model of $\epsilon_1(N)$ captures the essential features of the spectra arising from a generic model of USR achieved using a potential. The scalar power spectrum contains the signatures of USR such as the dip, followed by the rise of k^4 , and a peak amplitude. Since our model has an extended duration of SR after USR, the spectrum settles to another scale invariant regime past the peak. These individual features have been studied in several earlier works [46–48, 51–53, 55, 56, 60, 72–75].

As mentioned earlier, since we are interested in enhancing scalar power over small scales, the first phase of SR corresponds to the time when CMB scales exit the Hubble radius. The

² $M_{\text{Pl}} = \sqrt{\hbar c / (8\pi G)}$ is the reduced Planck mass in terms of the fundamental constants, the reduced Planck's constant \hbar , the speed of light c and the gravitational constant G .

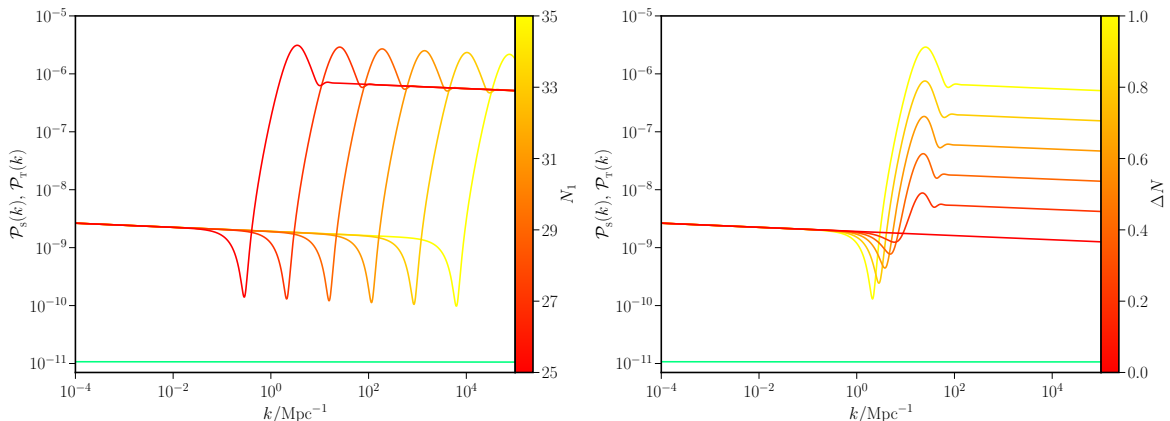


Figure 1. We present the behavior of scalar power spectra (in shades of red to yellow) arising from the parametric model of USR with variation of the two parameters of interest: the onset of USR N_1 (in the left panel, with constant $\Delta N = 1$) and the duration of USR ΔN (in the right panel, with constant $N_1 = 27$). The location of enhancement of scalar power is determined by N_1 with larger values implying enhancement over smaller scales. The amplitude of enhancement is determined by ΔN with large values implying larger enhancement. The range of parameters are chosen such that we preserve the nearly scale invariant behavior over $k \leq 0.1 \text{ Mpc}^{-1}$ and also ensuring that we do not violate the upper bound on enhancement due to CMB spectral distortions over scales around $k \simeq 10^4 \text{ Mpc}^{-1}$. The tensor power spectrum remains unaffected by the USR dynamics and stays the same across variation of parameters. It is displayed as a single horizontal green line.

dynamics of this phase is determined by the prefactor in the first term of Eq. (2.3), involving ϵ_1 and ϵ_2 . It is modelled to ensure proper values for the overall amplitude of the spectrum A_s , scalar spectral index n_s and tensor-to-scalar ratio r over scales exiting in the initial regime of SR. Further, we also restrict the range of variation of ΔN so that the enhancement does not violate the bound on $\mathcal{P}_s(k)$ due to spectral distortions in CMB around $k \simeq 10^4 \text{ Mpc}^{-1}$. As we vary the parameter N_1 we observe that feature of dip and rise shift across the range of wavenumber k , with larger values of N_1 shifting it to larger values of k . The increase in ΔN leads to increase in the amplitude of enhancement while also making the dip more prominent prior to the rise.

The tensor power spectrum remains nearly scale invariant throughout the range of scales, as it is largely unaffected by USR dynamics. However, they may suffer a step like drop in amplitude in case of models that have a brief rise in $\epsilon_1(N)$ just prior to the epoch of USR. Such models may even lead to an interruption in inflation if the rise in $\epsilon_1(N)$ crosses unity before decreasing rapidly during USR. These models are called punctuated inflationary models [76–79]. We do not include such a punctuation in our parametric model as we are mainly interested in the rise in the scalar power, though it can be included if required through an additional term in the parameterization (see Ref. [49] for such a reconstruction).

Based on our analysis, we obtain the following relation between the number of e-folds N_1 and the scale corresponding to the peak of the primordial power spectrum, k_{peak} (Figure 1). For $\Delta N = 0.2$,

$$N_1 \simeq 25 + \ln \left(\frac{k_{\text{peak}}}{3 \text{ Mpc}^{-1}} \right) \quad (2.9)$$

and

$$N_1 \simeq 25 + \ln \left(\frac{k_{\text{peak}}}{3.48 \text{ Mpc}^{-1}} \right) \quad (2.10)$$

for $\Delta N = 1$. From Fig. 1 it is clear that the power spectrum deviates significantly from the nearly scale invariant behavior over $k \gtrsim k_{\text{peak}}/10$.

We use this parametric model of USR and the associated numerical setup that computes scalar and tensor power spectra to compare against the datasets of CMB, galaxy surveys and Lyman- α . We shall discuss the methods and results of our analyses in the following sections.

3 Results

In this paper, we aim to constrain the deviation of a class of USR models from the standard model of slow roll inflation followed by Λ CDM evolution. Planck CMB temperature and polarization data puts strong constraints on such deviation at scales $10^{-3} \text{ Mpc}^{-1} \lesssim k \lesssim 0.2 \text{ Mpc}^{-1}$ ³. Lyman- α data at intermediate redshifts ($2 \lesssim z \lesssim 4$) can probe scales comparable to the Jeans' scales in IGM ($k_J \simeq 10 \text{ Mpc}^{-1}$). We consider Planck data and other related data sets at comparable scales, along with high spectral-resolution Lyman- α data in our analysis.

3.1 CMB and galaxy survey data

We consider the combined dataset of anisotropies in temperature and polarization of CMB from Planck 2018 and BICEP/KECK 2018 (BK18), along with galaxy survey dataset from BOSS and DES [80–83]. Given the sensitivity of the CMB data, we expect the strongest constraint on the model parameters from Planck data. Hence, we first compare the model against the data of Planck 2018 and BK18, and examine the constraints. We then extend the dataset to include BOSS and DES to study the improvement in the constraints. We use the publicly available package called CosmoMC to perform the comparison and Monte-Carlo sampling of the posterior distribution of parameters [84]. We modify the CAMB package within the setup of CosmoMC to incorporate the power spectra arising from the model of interest [85]. We use a modified version of a package called PBS⁴, which computes scalar and tensor power spectra for a given model of inflation, to implement the above mentioned alteration to CAMB in CosmoMC. Further, we use GetDist to marginalize along various dimensions in the parameter space and plot the resulting posterior distribution [86].

Since we are interested in studying the impact of enhanced scalar power on small scales, we set the priors on the parameters of interest as $N_1 = [25, 35]$ and $\Delta N = [0, 1]$. The parameter N_1 determines the location of the enhancement of the scalar power spectrum and the range of values that we have chosen corresponds to onset of enhancement over $k = [0.1, 10^5] \text{ Mpc}^{-1}$ ⁵.

The parameter ΔN affects both the location and amount of enhancement of the spectrum. Our choice of the range corresponds to relative enhancement of about $[0, 10^3]$ over the nearly scale-invariant amplitude. As noted in Sec. 2, we choose the range of ΔN such that we do not violate the upper bound on $\mathcal{P}_s(k) \lesssim 10^{-5}$ arrived at from the limit on spectral distortions obtained by FIRAS [64, 65, 87]. The amplitude of the scalar and tensor power over the large scales prior to enhancement is determined by H_i , ϵ_{1i} and ϵ_{2i} . Thus our inflationary

³The approximate smallest scale probed by Planck data corresponds to $k \simeq \ell/\eta_0$, where $\ell \simeq 2500$ and the conformal time at the present time $\eta_0 \simeq 11000 \text{ Mpc}$.

⁴It is developed by one of the authors and publicly available at <https://gitlab.com/ragavendrahv/pbs>.

⁵We should clarify we are not allowing for an epoch of USR at a much earlier time during inflation, which along with rescaling of the overall normalization, can suppress power over the largest scales probed by CMB, $k \simeq 10^{-4} \text{ Mpc}^{-1}$. In fact, it has been shown that such an epoch can mildly improve the fit to CMB [78, 79]. However, we are not allowing for this effect in our work and the priors on N_1 are chosen solely to explore only the small-scale enhancement due to a late epoch of USR.

Parameters	Minimum	Maximum
$\Omega_b h^2$	5×10^{-3}	0.10
$\Omega_c h^2$	10^{-3}	0.99
$100 \theta_{MC}$	0.50	10.00
τ	10^{-2}	0.80
$\log_{10}(H_i/M_{Pl})$	-5.40	-4.90
$\log_{10}(\epsilon_{1i})$	-4.25	-3.40
$\log_{10}(\epsilon_{2i})$	-2.50	-1.20
N_1	25.00	35.00
ΔN	0.00	1.00

Table 1. The priors on the cosmological parameters and those on our inflationary model parameters that are used while comparing the models against datasets of `Planck 2018`, `BK18`, `BOSS` and `DES` are listed. We have varied the inflationary parameters determining the power spectrum over large scale in logarithmic scale to explore a wide region in the parameter space.

model has five parameters and the priors on these five model parameters along with those on other cosmological parameters are given in Tab. 1.

3.1.1 Five parameter model

We first compare the model against the CMB datasets by using the likelihoods of `Planck2018` and `BK18`. We sample the posterior distribution and obtain the constraints on the marginalized distribution of the parameters of interest. We find that the four cosmological parameters, namely $\Omega_c h^2$, $\Omega_b h^2$, θ_{MC} and τ are constrained around the same value as they are in PL model. Besides, the constraints on H_i , ϵ_{1i} and ϵ_{2i} , are such that they lead to a nearly-scale invariant behavior over the CMB scales.

As to the parameters of `USR`, N_1 is bounded from below. To quantify this lower limit, we use `GetDist` which deals with one-sided distributions and sharp boundaries in the distribution using a linear boundary kernel estimator and suitable normalization [86]. We obtain that $27.26 < N_1 < 33.29$ at the level of $1\text{-}\sigma$ and $N_1 > 26.61$ at the level of $2\text{-}\sigma$. On the other hand, ΔN is unconstrained with a mild preference towards $\Delta N = 0$. To avoid clutter, we have not plotted the contours of the marginalized posterior distribution of this analysis and plot the distribution only for the following case.

Next, we extend the dataset to include galaxy surveys, i.e. `BOSS` and `DES` likelihoods and repeat the above exercise. We present the marginalized contours of the posterior distribution of this analysis in Fig. 2. We once again observe that the parameters such as $\Omega_c h^2$, $\Omega_b h^2$ get constrained around the same values as in the PL model. The onset of `USR` is constrained as $N_1 > 29.73$ at $1\text{-}\sigma$ level and $N_1 > 27.53$ at $2\text{-}\sigma$ level. ΔN is again unconstrained, though there is mild preference towards $\Delta N = 0$.

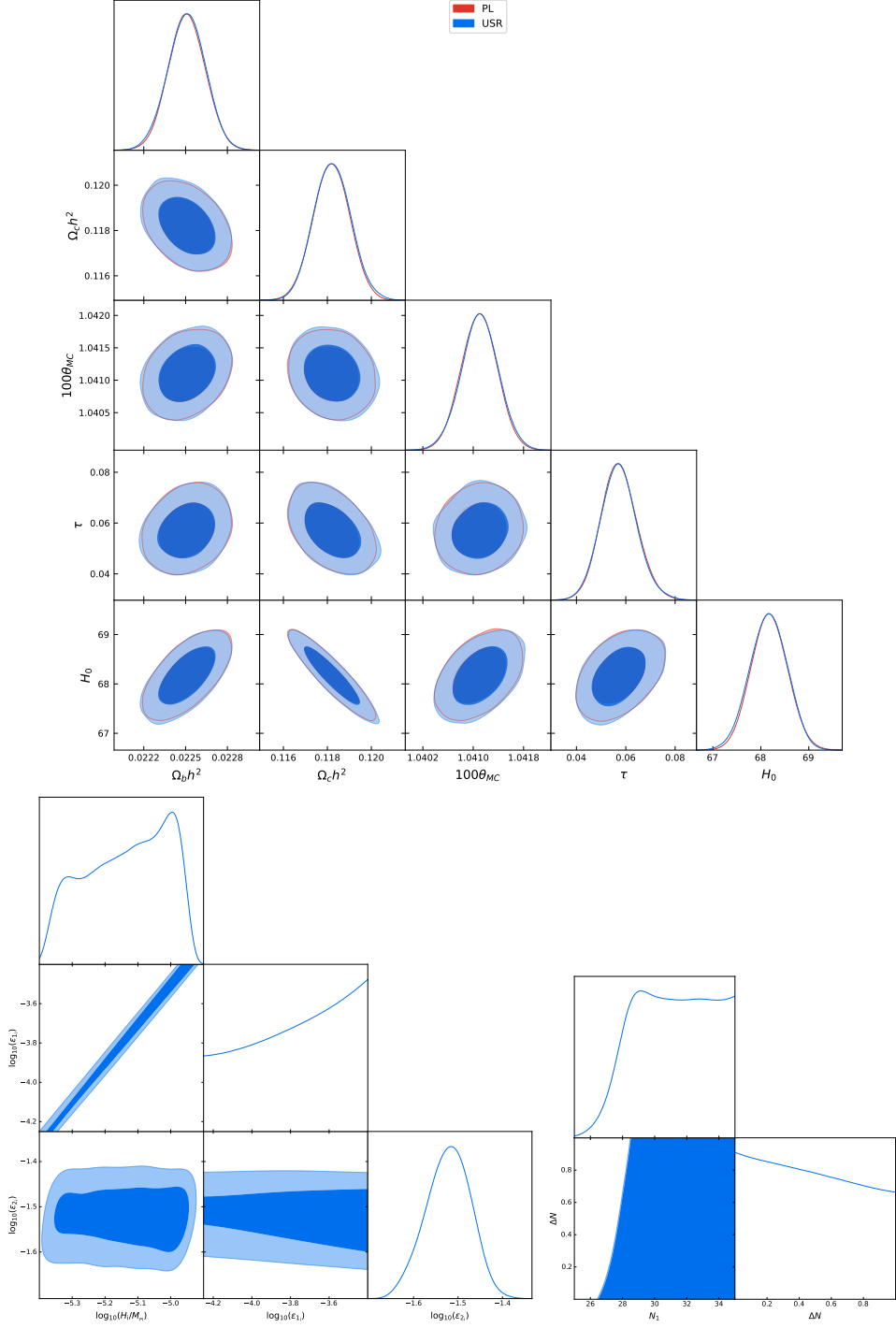


Figure 2. The $1\text{-}\sigma$ and $2\text{-}\sigma$ contours of the posterior distribution of the parameters of USR model when compared against CMB (Planck2018+BK18) and galaxy survey (BAO+DES) data are presented here. The standard cosmological parameters are presented (on the top panel). Their distributions are the essentially the same between PL and USR models. The three parameters that determine the spectrum on large scales, $\log_{10}(H_i/M_{\text{Pl}})$, $\log_{10}(\epsilon_1)$ and $\log_{10}(\epsilon_2)$, are presented (on bottom left) along with the parameters dictating USR epoch, N_1 and ΔN (on bottom right).

The constraints on the parameters H_i , ϵ_1 and ϵ_2 are similar to those obtained when

comparing against CMB alone. The marginalized contours of H_i , ϵ_{1_i} and ϵ_{2_i} can be understood through their relations to the conventional parameters that describe the spectrum over large scales, namely the amplitude of scalar power at pivot scale A_s , the spectral index of the scalar power spectrum n_s and the tensor-to-scalar ratio r . These parameters describe the shape and amplitude of the power spectra in the PL model [88]. Under slow roll approximation, which is valid over the initial slow roll regime of our model, we can relate our model parameters H_i , ϵ_{1_i} and ϵ_{2_i} to these PL parameters as (see, for example [69–71])

$$A_s \simeq \frac{H^2(N_p)}{8\pi^2 M_{\text{pl}}^2 \epsilon_1(N_p)}, \quad (3.1)$$

$$\simeq \frac{H_i^2}{8\pi^2 M_{\text{pl}}^2 \epsilon_{1_i}} e^{-\epsilon_{2_i} N_p}, \quad (3.2)$$

$$n_s \simeq 1 - 2\epsilon_1(N_p) - \epsilon_2(N_p), \quad (3.3)$$

$$\simeq 1 - 2\epsilon_{1_i} e^{\epsilon_{2_i} N_p} - \epsilon_{2_i}, \quad (3.4)$$

$$r \simeq 16\epsilon_1(N_p), \quad (3.5)$$

$$\simeq 16\epsilon_{1_i} e^{\epsilon_{2_i} N_p}. \quad (3.6)$$

The above quantities are evaluated at N_p , when the pivot scale k_p exits the Hubble radius, which we have set to be $N_p = 22$ as mentioned before. We have used the fact that the second slow-roll parameter is a constant ϵ_{2_i} during the initial slow roll regime and so $\epsilon_1(N_p) = \epsilon_{1_i} \exp(-\epsilon_{2_i} N_p)$ [cf. Eq. (2.3)]. Also, the Hubble parameter $H(N_p)$ can be evaluated by evolving it from its initial value H_i , as dictated by Eq. (2.5). However, the value of $\epsilon_1(N_p)$ is so small that it makes little difference to $H(N)$ during the evolution. Hence, we have assumed $H(N_p) \simeq H_i$.

However, we should note that we do not directly vary A_s , n_s or r while comparing our model against data. We vary the model parameters H_i , ϵ_{1_i} and ϵ_{2_i} , along with N_1 and ΔN , and numerically evolve the background and perturbations for each given value of them, when comparing against data. Hence, A_s , n_s or r are parameters derived from the model parameters H_i , ϵ_{1_i} and ϵ_{2_i} through the relations given above. We present the contours of these derived parameters in Fig. 3. The amplitude A_s being constrained corresponds to H_i being strongly correlated with ϵ_{1_i} . Note that A_s , n_s and r are exponentially sensitive to ϵ_{2_i} due to the time evolution of $\epsilon_1(N)$. Therefore, constraints on these three parameters, especially on n_s , correspond to the strong constraint on ϵ_{2_i} . The tensor-to-scalar ratio r being bound from above mainly translates to the unconstrained behavior of ϵ_{1_i} , as the range of prior on ϵ_{1_i} is well within the bound on r . Besides, the parameter r is also indirectly related to n_s , through its dependence on ϵ_{2_i} . Thus the closing of contour on r with a lower bound is due to a combination of the lower limit of the prior on ϵ_{1_i} and the tight constraint on ϵ_{2_i} . It is worth noting that, if it was parametrized as $r \simeq 16\epsilon_{1_i}$, neglecting the time evolution of ϵ_1 , we would have obtained only an upper bound and no lower bound on r .

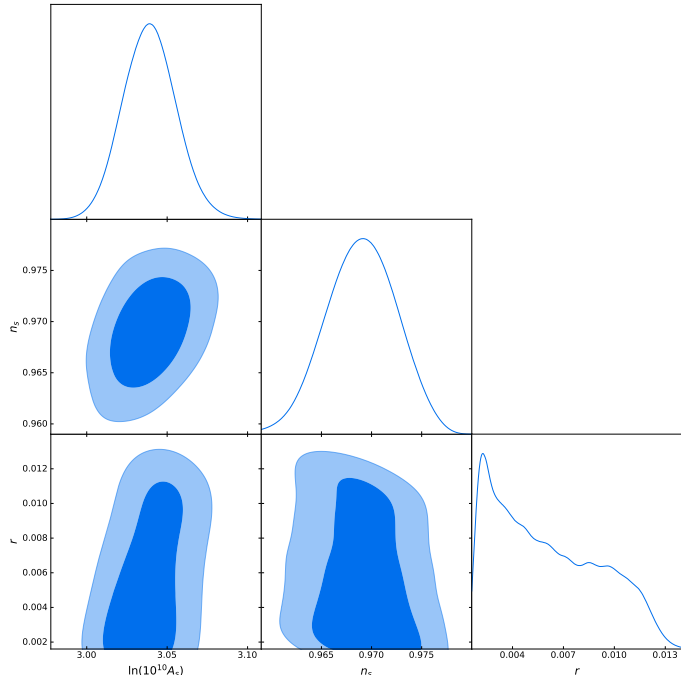


Figure 3. The $1\text{-}\sigma$ and $2\text{-}\sigma$ contours of the posterior distribution of the parameters A_s, n_s and r derived from H_i, ϵ_{1i} and ϵ_{2i} , using slow-roll approximation over the regime before the onset of USR, are presented here. The apparent closing of contour on r with a lower bound is due to the lower limit of the range of prior on ϵ_{1i} .

3.1.2 Two parameter model

An important takeaway from the above analyses is that the constraints on the parameters determining the first slow roll phase are largely independent of the USR parameters. This is because the slow-roll and USR dynamics are fairly independent of each other in our model and they affect different ranges of scales. To illustrate this point more clearly, we compare our model against the dataset of CMB and galaxy surveys, by varying just the USR parameters N_1 and ΔN , while fixing the other three parameters H_i, ϵ_{1i} and ϵ_{2i} at values well within their constraints as follows: $\log_{10}(H_i/M_{\text{Pl}}) = -5.14$, $\log_{10}(\epsilon_{1i}) = -3.82$ and $\log_{10}(\epsilon_{2i}) = -1.47$. We find that the constraints on N_1 and ΔN are very similar to those obtained in the previous analysis when we varied all the five model parameters. We obtain $N_1 > 29.85$ at $1\text{-}\sigma$ level and $N_1 > 27.56$ at $2\text{-}\sigma$ level, matching the bounds gotten earlier. ΔN is unconstrained as before with a mild preference towards zero.

However, the fixing of the inflationary three parameters reduces the computational time taken for sampling the posterior distribution, while still arriving at the correct constraints on USR parameters. This confirms the separation of scales between slow roll and USR dynamics. One can study the USR phase affecting the small scales while not altering much of the slow roll dynamics affecting the large scales and arrive at the same conclusion, as while considering the complete dynamics of our model.

We should also caution that there may be certain potentials realizing USR dynamics, where the parameters dictating USR may also affect the shape of spectra over large scales. Such potentials may typically lead to strong running of n_s as mentioned earlier. These effects can alter the fit to CMB and hence push the onset of USR further to a later time during inflation. Thus, our bounds on N_1 are relatively conservative in this regard.

The lower bound obtained on N_1 is an important result of these analyses so far. The bound at the level of $2\text{-}\sigma$ of $N_1 > 26.61$ from CMB is improved by about an e-fold as $N_1 > 27.56$ with addition of galaxy surveys to the dataset. It translates to an upper bound on \bar{N}_1 , the earliest onset of USR from the end of inflation. The bound of $N_1 > 27$ is simply $\bar{N}_1 < 45$, implying that USR can occur only in the last 45 e-folds of inflation. It essentially indicates the data's preference for the nearly scale-invariant spectrum up to scales $k \lesssim 1 \text{ Mpc}^{-1}$ and avoidance of any deviation such as a dip or rise over these scales. On the other hand, the indifference of data towards the range of ΔN suggests that an epoch of USR lasting for as long as 1 e-fold beyond $N_1 = 27$ and hence a relative enhancement as large as 10^3 past $k = 1 \text{ Mpc}^{-1}$ does not affect the fit of the model over large scales. We note that this scale is comparable to but smaller than our expectation based on the relation $k\eta_0 = \ell$, which follows from the property of spherical Bessel function. We note that for a given angular scale ℓ , the contribution from a linear scale $k < \ell/\eta_0$ falls very sharply. However, it only falls as $1/(k\eta_0)$ for $k > \ell/\eta_0$ (for details see e.g. [89]). This means CMB data is sensitive to much larger values of k for a fixed ℓ and η_0 as our results show.

3.2 Lyman- α forest

Lyman- α forest is the dense, ragged forest of lines seen in the spectra of the background quasars. These lines correspond to regions in the Inter-Galactic Medium (IGM) with HI column number density lying between the range: $N_{\text{HI}} = 10^{12} - 10^{15} \text{ atoms/cm}^2$. Hydrodynamical simulations identify these regions with underlying matter densities in the mildly non-linear range i.e. $\delta \leq 10$. It is known that Lyman- α forest can probe density perturbations on scales as small as the thermal Jeans' scale of IGM at intermediate redshifts ($k \simeq 10 \text{ Mpc}^{-1}$). Based on hydrodynamical simulation of Lyman- α forests, Murgia et al. [90] put constraints on a large range of models with matter power deficit as compared to the Λ CDM model. Most of the models we consider correspond to excess power as compared to the Λ CDM model. While it is tempting to use the results of [90] to constrain our models, the relevant cosmological observable in this case, the flux deficit, is a non-linear function of matter power and therefore we recompute these constraints based on a semi-analytic approach [91–95].

The semi-analytic modelling of Lyman- α has been used to constrain cosmological models which either have excess or reduced matter power in [94, 95]. In this approach, the observed redshift evolution of effective optical depth of Lyman- α forest, based on high spectral-resolution data [66], is used.

To constrain our model against the Lyman- α data, we define and use the relative difference between the 1D baryonic power spectra of the models of interest $\mathcal{P}_b^{1D}(k)$ and the standard Λ CDM evolution following slow-roll inflation leading to a power-law primordial power spectrum $\mathcal{P}_b^{1D}(k)|_{\text{PL}}$. The 1D baryonic power spectrum can be defined in terms of the 3D baryonic power spectrum $P_b^{(3)}(k, z)$ as (e.g. [91, 92] for details):

$$P_b^{(1)}(k, z) = \frac{1}{2\pi} \int_{|k|}^{\infty} k' P_b^{(3)}(k', z) dk' \quad (3.7)$$

with

$$P_b^{(3)}(k, z) = \frac{P_m^{(3)}(k)}{[1 + (k/k_J)^2]^2}, \quad (3.8)$$

and the Jeans wavenumber k_J is:

$$k_J = H_0 \left[\frac{2\gamma k_B T_0}{3\mu m_p \Omega_m (1+z)} \right]^{-1/2}, \quad (3.9)$$

where the parameters have their usual meaning, with $\mu = 0.6$. For the standard choice of parameters, we have $k_J \simeq 8.5 h \text{ Mpc}^{-1}$ at the redshift $z = 3$.

We further average the relative difference $\Delta_m^{1D}(k)$ between 1D baryonic power spectra over the range of k . This allows us to define Δ_m^{1D} as follows:

$$\begin{aligned} \Delta_m^{1D}(k, z) &= \frac{\mathcal{P}_b^{1D}(k, z) - \mathcal{P}_b^{1D}(k, z)|_{\text{PL}}}{\mathcal{P}_b^{1D}(k, z)|_{\text{PL}}}, \\ \Delta_m^{1D}(z) &= \frac{1}{\int d \ln k} \int d \ln k \Delta_m^{1D}(k, z). \end{aligned} \quad (3.10)$$

We note that $\Delta_m^{1D}(z)$ is a function of redshift owing to the evolution of Jeans scale (Eq. (3.9)). To parameterize the relative difference, $\Delta_m^{1D}(z)$ is computed at the redshift of $z_* = 2.2$. The choice of z_* has no impact on our main results. The range of integration over k is taken to be $[10^{-5}, 10^3] \text{ Mpc}^{-1}$ to arrive at $\Delta_m^{1D}(z_*)$. Our approach is similar to Murgia et al. (2017) [90] where the deviation from the standard 1D power spectrum is quantified and compared against data. We differ from the measure used by [90] in using baryonic power spectra and using a larger range of k to define the relative difference between the standard and modified models. We use a semi-analytic model for probing the thermal, dynamical and ionization state of the Lyman- α clouds at higher redshifts using the following parameters: J_0 (the intensity of hydrogen-ionizing photons), T_0 (the temperature of the IGM), γ (the equation of state of the Lyman- α clouds) (for details see [95] and references therein). Based on observational data and hydrodynamical simulations, these parameters are varied in the following range: $7000 \leq T_0 \leq 15000 \text{ K}$, $0.7 \times 10^{-12} \text{ sec}^{-1} < J_0 < 2 \times 10^{-12} \text{ sec}^{-1}$, and $0.9 \leq \gamma \leq 2.2$ (for details see [95]). In addition, two cosmological parameters, N_1 and ΔN , denoting the modified small scale power owing to USR phase, are included in the analysis.

We have simulated the 1D density and velocity field using lognormal distribution in the redshift interval $2 \leq z \leq 4.2$ at uniform redshift intervals of $\Delta z = 0.1$ for comparison with data. The Lyman- α effective optical depth $\tau_{\text{eff}}(z)$ is defined as: $\tau_{\text{eff}}(z) = -\log [\langle \exp(-\tau) \rangle]$. From the standpoint of observation, the ensemble average (represented by the angular brackets $\langle \dots \rangle$) is substituted by the average over the number of individual Lyman- α clouds at a particular redshift: $\tau_{\text{eff}}(z) = -\log [\sum_i \exp(-\tau_i) / N]$, where N is the number of the simulated Lyman- α clouds at a redshift z , and τ_i denotes the optical depth of the i -th Lyman- α cloud at that redshift.

In Fig. 4, we plot the evolution of τ_{eff} along with the data. To understand the evolution of τ_{eff} , we first discuss two extreme cases. If $\tau_i \ll 1$ for all clouds, then $\tau_{\text{eff}} \propto (1+z)^{4.5}$, which is the expected evolution of the Gunn-Peterson optical depth for the background universe. In the other extreme case, if $\tau_i \gg 1$, then τ_{eff} is independent of τ_i and hence of redshift. The observed behaviour lies between these two extremes which shows that many clouds are making transition from optical thin to optically thick as redshift increases. ($\tau_i = N_{\text{HI}} \sigma_\alpha$, where σ_α is the cross-section of Lyman-alpha scattering. The line center cross-section $\simeq 5 \times 10^{-14} \text{ cm}^{-2}$ for $T_0 \simeq 10^4$.) The data fits the Λ CDM model well and can be used to constrain models with deficit or excess power [94]. Fig. 4 shows the redshift evolution of τ_{eff} get flatter as the matter power is increased. This is expected as a larger fraction of Lyman- α clouds become optically thick at higher redshift as the matter power is increased. This demonstrates that the slope of the τ_{eff} evolution is a robust probe of matter power (for further details see [94, 95] for cases analysing both deficit and excess of power). However, the effective optical depth is also affected by parameters used to model the ionization and thermal state of clouds. In particular, the increase in matter power is degenerate with ionizing intensity J_0 and partially degenerate

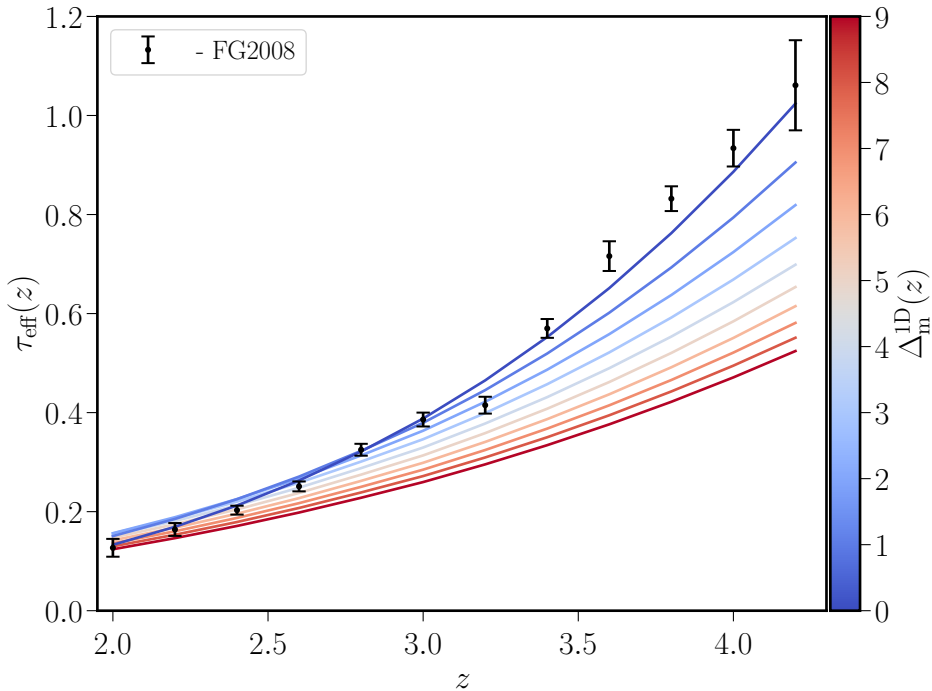


Figure 4. The evolution of τ_{eff} is shown based on our model predictions along with the high spectral-resolution data (in black dots along with error bars, FG2008) [66]. Different curves (from top to bottom) correspond to increasing average relative difference of 1D power spectrum $\Delta_m^{1D}(z)$ [cf. Eq. (3.10)] (in shades of blue to red). In simulating the evolution of $\tau_{\text{eff}}(z)$ for different values of $\Delta_m^{1D}(z)$, the Lyman- α parameters have been held fixed to the following values: $J_0 = 10^{-12} \text{ s}^{-1}$, $T_0 = 2.3 \times 10^4 \text{ K}$ and $\gamma = 0.7$.

with T_0 and γ (see [95] for details). Therefore, the magnitude of the change of matter power that can be probed by the data depends on the prior information on these parameters. We discuss the priors on these parameters above. These correspond to the widest possible priors on these parameters from the literature. Based on our analysis of the simulated data, we find that these priors constrain the change in the 1D matter power spectrum to be smaller than roughly a factor of five. For narrower priors, the constraints are stronger. If the results of [90] are directly applied to our case, the change in the matter power is constrained to be less than approximately 50%.

In Fig. 5, we present the constraints from Lyman- α data as a color gradient map with contours based on the deviation measure, $\Delta_m^{1D}(z_*)$, in the N_1 - ΔN plane. The contours denoting the values of $\Delta_m^{1D}(z_*) = 1, 5$ and 10 are displayed. The region above these contours is ruled out. To understand these constraints, we show models corresponding to two values of $\Delta_m^{1D}(z_*)$ in Fig. 6. In Fig. 5 we also plot a curve corresponding to $\Delta_m^{1D}(z_*) = 0$. This curve demarcates the region of positive deviation from negative deviation. The negative deviation is caused by 1-D spectrum getting suppressed by the dip in matter power and the subsequent rise suppressed by the cutoff at Jean's scale [cf. Eq. (3.8)]. However, all the spectra that we consider (Fig. 6) yield only a small negative deviation, $|\Delta_m^{1D}(z_*)| \leq 10^{-2}$. The data is insensitive to such small deviation and therefore cannot probe the interplay between the dip and subsequent rise in the matter power (Fig. 6). Fig. 5 implies that significant duration of USR $\Delta N \geq 0.5$, can occur only for $N_1 > 31$, or equivalently $\bar{N}_1 < 41$. This means that

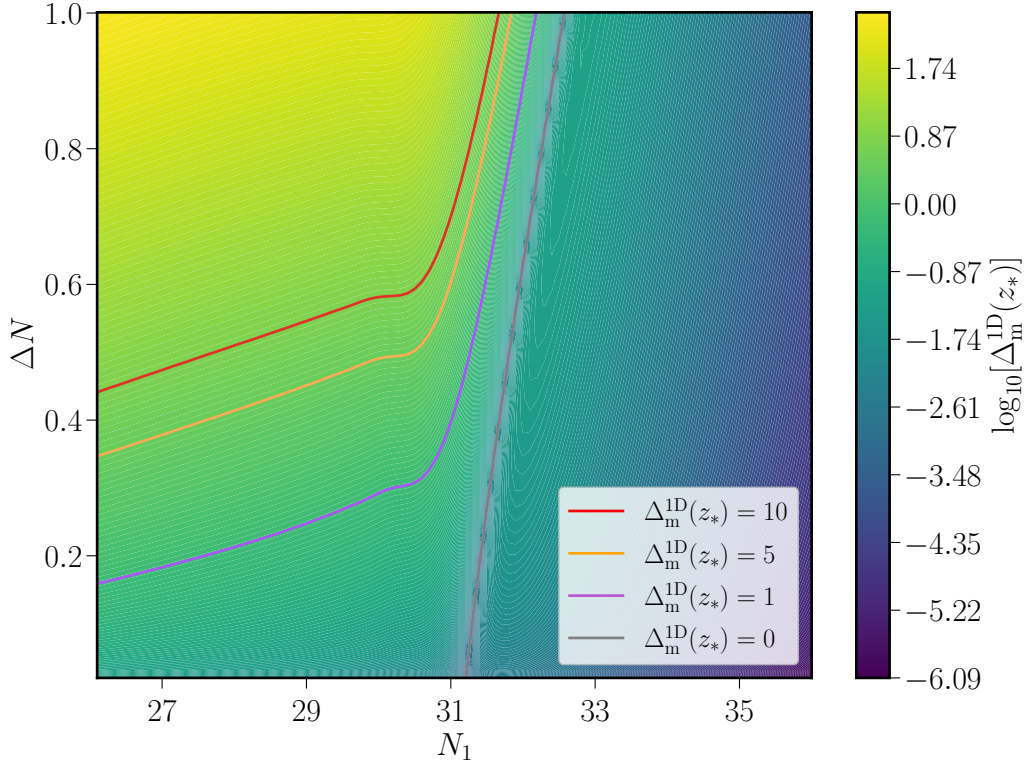


Figure 5. We present the density plot of the average relative difference of the 1D matter power spectrum of the USR model with respect to the standard power law power spectrum $\Delta_m^{1D}(z_*)$ [Eq. (3.10)], as a function of N_1 and ΔN (in shades of blue to green). We have also highlighted the contours corresponding to $\Delta_m^{1D}(z_*) = 10, 5, 1$ and 0 (with lines in red, orange, violet and grey respectively). In the region to the right of the line corresponding to $\Delta_m^{1D}(z_*) = 0$, the parameters lead to $\Delta_m^{1D}(z_*)$ being small and negative in value.

substantial rise in power can occur only at $k \geq 10^2 \text{ Mpc}^{-1}$.

We can understand our results using Eqs. (3.8), (3.7), and (3.9). In the usual ΛCDM model based on PL power spectra from slow roll inflationary models, the three-dimensional matter power spectrum scales as $k^{-3}(\log(k))^2$ at small scales (see e.g. [89]). For $k \lesssim k_J$, the baryonic 1D power spectrum scales as $k^{-1}(\log(k))^2$ and for $k > k_J$, $P_b^{(1)}(k, z) \propto k^{-5}(\log(k))^2$. In the USR models, the increase in the primordial power spectrum can scale as k^4 (e.g. Fig. 1). This means the main contribution to the enhanced power comes from scales $k \lesssim k_J \simeq 10 \text{ Mpc}^{-1}$ as the 1D baryonic power spectrum scales as $k(\log(k))^2$ for $k < k_J$. However, for $k > k_J$ the decrement in 1D power spectrum is shallow ($P_b^{(1)}(k, z) \propto k^{-1}(\log(k))^2$) and we expect non-negligible contribution from smaller scales. Our analysis suggests scales up to 10 times smaller than $k = k_J$ can be constrained in USR models as the 1D power spectrum falls by only a factor of two in this range: $P_b^{(1)}(100, z)/P_b^{(1)}(10, z) \simeq 0.5$.

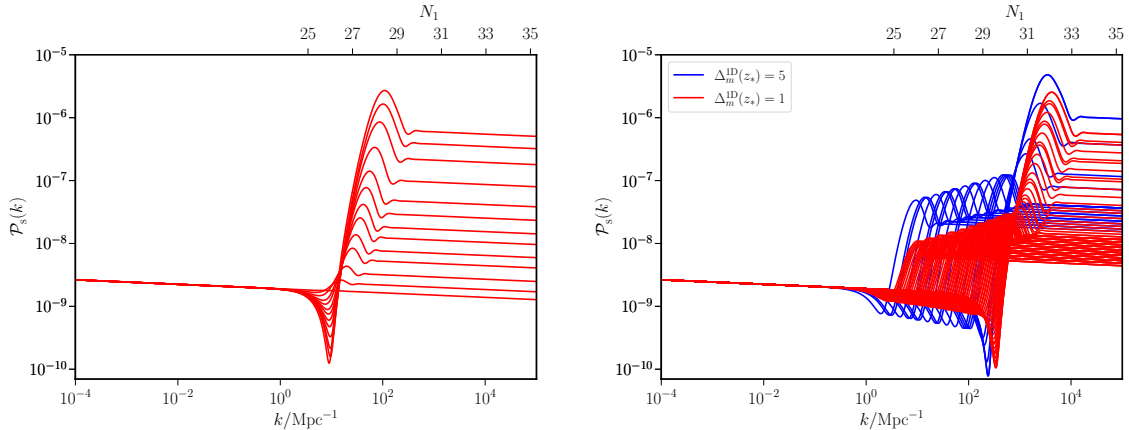


Figure 6. Left Panel: The scalar power spectra based on $2\text{-}\sigma$ bound on parameters N_1 and ΔN from CMB and galaxy surveys (Planck2018+BK18+BOSS+DES) are shown (cf. Fig. 2). Right Panel: The scalar power spectra corresponding to constraints from Lyman- α data are displayed. The scalar power spectra leading to $\Delta_m^{1D}(z_*) = 1$ and $\Delta_m^{1D}(z_*) = 5$ are presented (in red and blue respectively). These spectra are obtained from the values of N_1 and ΔN along the respective contours in Fig. 5. The upper x-axis displays N_1 corresponding to the location of the peak, k_{peak} , in the spectrum. It is obtained using the relation: $N_1 \simeq 25 + \ln(k_{\text{peak}}/\text{Mpc}^{-1}) - \ln(3.48)$ [cf. Eq. (2.10)].

4 Conclusion

Recent LIGO and PTA discoveries have opened the possibility of enhanced scalar power at small scales. This enhancement can be achieved by a brief USR phase during the inflationary era. In this paper, we aim to detect/constrain the dynamics of this phase of inflation using cosmological data. In particular, we use CMB data owing to its unprecedented precision and Lyman- α data as it is sensitive to small scales. We parameterize our models to determine the onset of the USR phase during inflation and the deviation of the matter power as compared to the power-law model.

From CMB and other data at comparable scales, we find that the earliest onset of USR can only be $\bar{N}_1 \lesssim 45$ (Fig. 2). With Lyman- α dataset, the onset gets pushed further to $\bar{N}_1 \lesssim 41$ (Fig. 5). The duration ΔN is largely unconstrained from CMB and other datasets. But Lyman- α strongly constrains the duration to be $\Delta N \lesssim 0.4$ along with $\bar{N}_1 < 41$. These constraints limit the possibility of having any appreciable epoch of USR only to the last 41 e-folds of inflation. This implies a constraint on the amplitude of $\mathcal{P}_s(k) < 10^{-7}$ over $0.1 < k/\text{Mpc}^{-1} < 10^2$. Such a constraint is a considerable improvement of about two orders of magnitude on the bound on $\mathcal{P}_s(k)$ compared to the limit from FIRAS over these scales [87].

In Fig. 6, we plot the range of power spectra that are allowed by different data sets. In Fig. 7, we present our constraints in terms of the primordial power spectrum and wavenumber, which is more readily connected to cosmological observables and can be compared to other constraints such as spectral distortion. This helps us see the improvement in the constraint on the amplitude of power by Lyman- α data over spectral distortion for $k \lesssim 10^2 \text{Mpc}^{-1}$. We should add that the exact shape of the bounds, especially the blue lines corresponding to Lyman- α constraints in Fig. 7, are dictated to some extent by the shape of the spectrum in the USR model of interest (e.g. [96–99] for similar constraints but for different models of dark matter and specific parameterized forms of the primordial power spectra.).

In light of our constraint on the onset of USR, we should remark about the implications

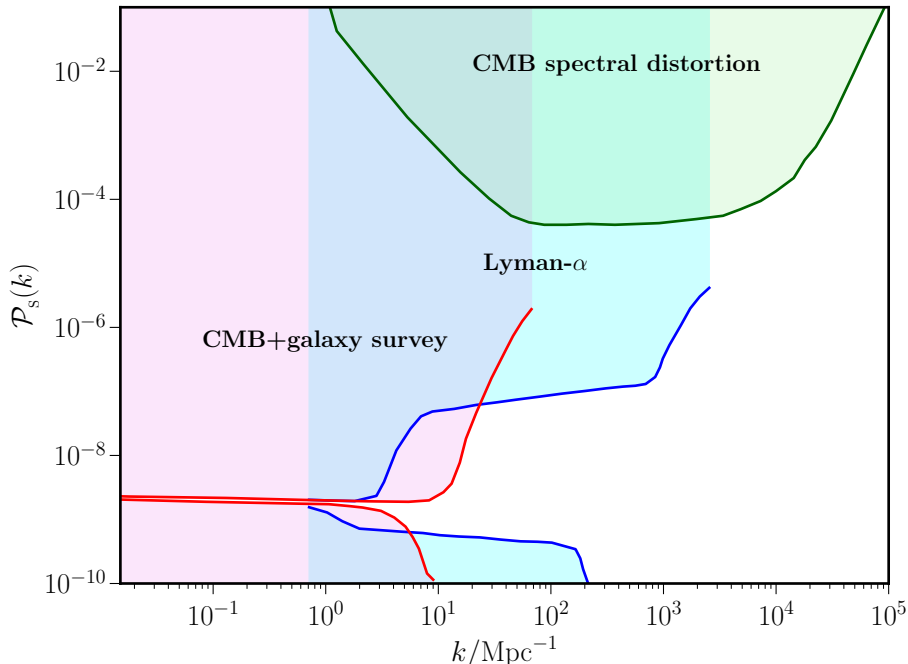


Figure 7. The constraints shown in Fig. 6 are displayed in $\mathcal{P}_s(k)$ - k plane. The red and blue lines correspond to CMB+galaxy surveys and Lyman- α data, respectively. The region bounded by these lines, e.g. narrow band around $\mathcal{P}_s(k) \simeq 2 \times 10^{-9}$, is allowed. The red lines demarcating the allowed region correspond to the envelopes of power spectra presented in the left panel of Fig. 6, which in turn is obtained from the $2\text{-}\sigma$ contour in the N_1 - ΔN plane in Fig. 2. The blue lines bounding the allowed region are the envelopes of power spectra presented in the right panel of Fig. 6. We have taken the set of spectra which lead to an average relative difference $\Delta_m^{\text{1D}}(z_*) = 5$. The three bands, from left to right, correspond to the region of spectrum ruled out by CMB+galaxy surveys data (lighter shade of red), both CMB+galaxy surveys and Lyman- α (in light blue), and just by Lyman- α data (shaded in cyan). We also display the constraints from CMB spectral distortion (green lines bounding the region in lighter shade of green) [87].

of USR phase for other cosmological datasets and the possibility of extending these constraints using future observations.

1. As mentioned earlier, the dip in the tree-level power spectrum prior to rise is a unique signature of USR models. In an earlier work, it was shown that this dip could be gleaned in the spectrum of 21-cm signals from the Dark Ages [53]. Due to the constraint that we have obtained on \bar{N}_1 and ΔN , if the dip were to occur at $k \simeq 10 \text{ Mpc}^{-1}$, it shall be shallower, with the amplitude at the lowest point within an order of magnitude of the nearly scale-invariant behavior. Else it may occur deeper but only at $k \geq 10^2 \text{ Mpc}^{-1}$. Besides, the loop-level contributions that may alter the shape of the dip may also exhibit their impact at such smaller scales [54].
2. To constrain the onset of USR at even smaller scales, one needs to explore possible future constraints due to spectral distortions over the scales of $10^4 \text{ Mpc}^{-1} \lesssim k \lesssim 10^6 \text{ Mpc}^{-1}$. We have already accounted for the constraint due to FIRAS on $\mathcal{P}_s(k) \lesssim 10^{-5}$ by restricting the range of duration of USR to be $\Delta N < 1$. But an upcoming mission like PIXIE with sensitivity as strong as $\mathcal{P}_s(k) \sim 10^{-8}$ can strengthen our constraints on \bar{N}_1

and ΔN [100]. Conversely the detection of spectral distortion of such levels, could be a confirmation of a brief USR phase.

3. As noted in the foregoing, there have been attempts to explain the stochastic GWs detected by PTA using USR models [19, 20, 25]. A scalar power spectrum that is required to induce such a secondary GW spectrum should have its steep rise in power between 10^5 – 10^7 Mpc^{-1} . This in turn corresponds to a phase of USR beginning at about $\bar{N}_1 \leq 32$. Such a value is still in the viable range of \bar{N}_1 as per the bounds we have obtained. If the signal by PTA is indeed due to USR, then it provides a crucial insight into the onset and duration of USR phase during inflation. However, we should caution that such a steep enhancement in power is beget along with strong scalar non-Gaussianity, captured in a non-trivial behavior in the associated non-Gaussianity parameter f_{NL} [45]. One needs to be careful in accounting for the non-Gaussian contributions to Ω_{GW} while comparing USR models against GW datasets [101–118].
4. The discovery of many high-redshift galaxies with unusually high stellar mass by JWST (e.g. [119, 120]) could be pointing at cosmological models with more power at small scales as compared to the Λ CDM model. However, it is also likely that the observed behaviour is owing to much higher star formation efficiency at high redshifts with significant contribution from population III stars (e.g. [119] and references therein). This issue is still being debated and remains unsettled.

In this paper, we consider the tree-level contribution to the primordial power spectrum. For USR models, there is ongoing discussion in the literature about the possibility of higher-order (loop-level) contribution dominating over the tree-level primordial power spectrum (e.g. [121–128] and [129–132] for counter claims). Within the framework of this ongoing debate, such an effect is possible only in the following cases: (i) the transitions between SR and USR are near-instantaneous and (ii) the enhancement in power is such that $\mathcal{P}_s(k) \sim 10^{-2}$, as required in the context of production of PBHs. This is not the case in our model as the transitions are not instantaneous, but smooth as is the case in any realistic model of USR driven by a smooth potential. Also, the range of ΔN we have worked with is restricted such that the maximum amplitude of $\mathcal{P}_s(k) \leq 10^{-5}$ as we do not violate the bound due to spectral distortion. Hence, the argument of loop-level spectrum dominating over tree-level spectrum does not occur in our analysis.

Acknowledgements

The authors thank Guillem Domènech and Ujjwal Kumar Upadhyay for useful comments and discussion. The authors acknowledge the usage of high-performance computing cluster at Raman Research Institute for various numerical computations. HVR thanks Raman Research Institute for support through postdoctoral fellowship.

References

- [1] O. Özsoy and G. Tasinato, *Inflation and Primordial Black Holes*, *Universe* **9** (2023), no. 5 203, [[arXiv:2301.03600](#)].
- [2] G. Domènech, *Scalar Induced Gravitational Waves Review*, *Universe* **7** (2021), no. 11 398, [[arXiv:2109.01398](#)].

- [3] **LISA Cosmology Working Group** Collaboration, E. Bagui et al., *Primordial black holes and their gravitational-wave signatures*, [arXiv:2310.19857](#).
- [4] **LIGO Scientific, Virgo** Collaboration, B. P. Abbott et al., *GWTC-1: A Gravitational-Wave Transient Catalog of Compact Binary Mergers Observed by LIGO and Virgo during the First and Second Observing Runs*, *Phys. Rev. X* **9** (2019), no. 3 031040, [[arXiv:1811.12907](#)].
- [5] **LIGO Scientific, VIRGO** Collaboration, R. Abbott et al., *GWTC-2.1: Deep Extended Catalog of Compact Binary Coalescences Observed by LIGO and Virgo During the First Half of the Third Observing Run*, [arXiv:2108.01045](#).
- [6] **LIGO Scientific, VIRGO, KAGRA** Collaboration, R. Abbott et al., *GWTC-3: Compact Binary Coalescences Observed by LIGO and Virgo During the Second Part of the Third Observing Run*, [arXiv:2111.03606](#).
- [7] **NANOGrav** Collaboration, G. Agazie et al., *The NANOGrav 15 yr Data Set: Evidence for a Gravitational-wave Background*, *Astrophys. J. Lett.* **951** (2023), no. 1 L8, [[arXiv:2306.16213](#)].
- [8] **EPTA, InPTA:** Collaboration, J. Antoniadis et al., *The second data release from the European Pulsar Timing Array - III. Search for gravitational wave signals*, *Astron. Astrophys.* **678** (2023) A50, [[arXiv:2306.16214](#)].
- [9] S. Bird, I. Cholis, J. B. Muñoz, Y. Ali-Haïmoud, M. Kamionkowski, E. D. Kovetz, A. Raccanelli, and A. G. Riess, *Did LIGO detect dark matter?*, *Phys. Rev. Lett.* **116** (2016), no. 20 201301, [[arXiv:1603.00464](#)].
- [10] M. Sasaki, T. Suyama, T. Tanaka, and S. Yokoyama, *Primordial Black Hole Scenario for the Gravitational-Wave Event GW150914*, *Phys. Rev. Lett.* **117** (2016), no. 6 061101, [[arXiv:1603.08338](#)]. [erratum: *Phys. Rev. Lett.*121,no.5,059901(2018)].
- [11] V. De Luca, G. Franciolini, P. Pani, and A. Riotto, *Primordial Black Holes Confront LIGO/Virgo data: Current situation*, *JCAP* **06** (2020) 044, [[arXiv:2005.05641](#)].
- [12] K. Jedamzik, *Primordial Black Hole Dark Matter and the LIGO/Virgo observations*, *JCAP* **09** (2020) 022, [[arXiv:2006.11172](#)].
- [13] K. Jedamzik, *Consistency of Primordial Black Hole Dark Matter with LIGO/Virgo Merger Rates*, *Phys. Rev. Lett.* **126** (2021), no. 5 051302, [[arXiv:2007.03565](#)].
- [14] Z.-C. Chen and A. Hall, *Confronting primordial black holes with LIGO-Virgo-KAGRA and the Einstein Telescope*, [arXiv:2402.03934](#).
- [15] **NANOGrav** Collaboration, A. Afzal et al., *The NANOGrav 15 yr Data Set: Search for Signals from New Physics*, *Astrophys. J. Lett.* **951** (2023), no. 1 L11, [[arXiv:2306.16219](#)].
- [16] Y.-F. Cai, X.-C. He, X.-H. Ma, S.-F. Yan, and G.-W. Yuan, *Limits on scalar-induced gravitational waves from the stochastic background by pulsar timing array observations*, *Sci. Bull.* **68** (2023) 2929–2935, [[arXiv:2306.17822](#)].
- [17] S. Vagnozzi, *Inflationary interpretation of the stochastic gravitational wave background signal detected by pulsar timing array experiments*, *JHEAp* **39** (2023) 81–98, [[arXiv:2306.16912](#)].
- [18] S. Choudhury, *Single field inflation in the light of Pulsar Timing Array Data: Quintessential interpretation of blue tilted tensor spectrum through Non-Bunch Davies initial condition*, *Eur. Phys. J. C* **84** (2024) 278, [[arXiv:2307.03249](#)].
- [19] H. Firouzjahi and A. Talebian, *Induced gravitational waves from ultra slow-roll inflation and pulsar timing arrays observations*, *JCAP* **10** (2023) 032, [[arXiv:2307.03164](#)].
- [20] B. Das, N. Jaman, and M. Sami, *Gravitational wave background from quintessential inflation and NANOGrav data*, *Phys. Rev. D* **108** (2023), no. 10 103510, [[arXiv:2307.12913](#)].
- [21] L. Liu, Z.-C. Chen, and Q.-G. Huang, *Probing the equation of state of the early Universe with*

- pulsar timing arrays*, *JCAP* **11** (2023) 071, [[arXiv:2307.14911](#)].
- [22] J. Ellis, M. Fairbairn, G. Franciolini, G. Hütsi, A. Iovino, M. Lewicki, M. Raidal, J. Urrutia, V. Vaskonen, and H. Veermäe, *What is the source of the PTA GW signal?*, *Phys. Rev. D* **109** (2024), no. 2 023522, [[arXiv:2308.08546](#)].
- [23] M. R. Gangopadhyay, V. V. Godithi, K. Ichiki, R. Inui, T. Kajino, A. Manusankar, G. J. Mathews, and Yogesh, *Is the NANOGrav detection evidence of resonant particle creation during inflation?*, [arXiv:2309.03101](#).
- [24] Q. Fei, *Constraints on the primordial curvature power spectrum by pulsar timing array data: a polynomial parameterization approach*, *Commun. Theor. Phys.* **76** (2024), no. 1 015404, [[arXiv:2310.17199](#)].
- [25] S. Choudhury, A. Karde, S. Panda, and M. Sami, *Realisation of the ultra-slow roll phase in Galileon inflation and PBH overproduction*, [arXiv:2401.10925](#).
- [26] Z.-C. Chen and L. Liu, *Can we distinguish the adiabatic fluctuations and isocurvature fluctuations with pulsar timing arrays?*, [arXiv:2402.16781](#).
- [27] A. A. Starobinsky, *Spectrum of adiabatic perturbations in the universe when there are singularities in the inflation potential*, *JETP Lett.* **55** (1992) 489–494.
- [28] D. K. Hazra, M. Aich, R. K. Jain, L. Sriramkumar, and T. Souradeep, *Primordial features due to a step in the inflaton potential*, *JCAP* **10** (2010) 008, [[arXiv:1005.2175](#)].
- [29] J. Martin, L. Sriramkumar, and D. K. Hazra, *Sharp inflaton potentials and bi-spectra: Effects of smoothing the discontinuity*, *JCAP* **09** (2014) 039, [[arXiv:1404.6093](#)].
- [30] J. Garcia-Bellido and E. Ruiz Morales, *Primordial black holes from single field models of inflation*, *Phys. Dark Univ.* **18** (2017) 47–54, [[arXiv:1702.03901](#)].
- [31] C. Germani and T. Prokopec, *On primordial black holes from an inflection point*, *Phys. Dark Univ.* **18** (2017) 6–10, [[arXiv:1706.04226](#)].
- [32] G. Ballesteros and M. Taoso, *Primordial black hole dark matter from single field inflation*, *Phys. Rev. D* **97** (2018), no. 2 023501, [[arXiv:1709.05565](#)].
- [33] J. M. Ezquiaga, J. Garcia-Bellido, and E. Ruiz Morales, *Primordial Black Hole production in Critical Higgs Inflation*, *Phys. Lett.* **B776** (2018) 345–349, [[arXiv:1705.04861](#)].
- [34] F. Bezrukov, M. Pauly, and J. Rubio, *On the robustness of the primordial power spectrum in renormalized Higgs inflation*, *JCAP* **02** (2018) 040, [[arXiv:1706.05007](#)].
- [35] M. Drees and Y. Xu, *Overshooting, Critical Higgs Inflation and Second Order Gravitational Wave Signatures*, *Eur. Phys. J. C* **81** (2021), no. 2 182, [[arXiv:1905.13581](#)].
- [36] V. Atal, J. Garriga, and A. Marcos-Caballero, *Primordial black hole formation with non-Gaussian curvature perturbations*, *JCAP* **09** (2019) 073, [[arXiv:1905.13202](#)].
- [37] S. S. Mishra and V. Sahni, *Primordial Black Holes from a tiny bump/dip in the Inflaton potential*, *JCAP* **04** (2020) 007, [[arXiv:1911.00057](#)].
- [38] G. Ballesteros, J. Rey, M. Taoso, and A. Urbano, *Primordial black holes as dark matter and gravitational waves from single-field polynomial inflation*, [arXiv:2001.08220](#).
- [39] K. Kefala, G. P. Kodaxis, I. D. Stamou, and N. Tetradis, *Features of the inflaton potential and the power spectrum of cosmological perturbations*, *Phys. Rev. D* **104** (2021), no. 2 023506, [[arXiv:2010.12483](#)].
- [40] M. Braglia, D. K. Hazra, F. Finelli, G. F. Smoot, L. Sriramkumar, and A. A. Starobinsky, *Generating PBHs and small-scale GWs in two-field models of inflation*, *JCAP* **08** (2020) 001, [[arXiv:2005.02895](#)].
- [41] R. Zheng and T. Q. Shi, Jiaming and, *On primordial black holes and secondary gravitational*

waves generated from inflation with solo/multi-bumpy potential *, *Chin. Phys. C* **46** (2022), no. 4 045103, [[arXiv:2106.04303](#)].

- [42] M. Braglia, A. Linde, R. Kallosh, and F. Finelli, *Hybrid α -attractors, primordial black holes and gravitational wave backgrounds*, *JCAP* **04** (2023) 033, [[arXiv:2211.14262](#)].
- [43] H.-R. Zhao, Y.-C. Liu, J.-X. Zhao, and N. Li, *The evolution of the primordial curvature perturbation in the ultraslow-roll inflation*, *Eur. Phys. J. C* **83** (2023), no. 9 783.
- [44] S. Choudhury, A. Karde, S. Panda, and M. Sami, *Scalar induced gravity waves from ultra slow-roll Galileon inflation*, [[arXiv:2308.09273](#)].
- [45] H. V. Ragavendra and L. Sriramkumar, *Observational Imprints of Enhanced Scalar Power on Small Scales in Ultra Slow Roll Inflation and Associated Non-Gaussianities*, *Galaxies* **11** (2023), no. 1 34, [[arXiv:2301.08887](#)].
- [46] C. T. Byrnes, P. S. Cole, and S. P. Patil, *Steepest growth of the power spectrum and primordial black holes*, *JCAP* **06** (2019) 028, [[arXiv:1811.11158](#)].
- [47] H. Motohashi, S. Mukohyama, and M. Oliosi, *Constant Roll and Primordial Black Holes*, *JCAP* **03** (2020) 002, [[arXiv:1910.13235](#)].
- [48] G. Tasinato, *An analytic approach to non-slow-roll inflation*, *Phys. Rev. D* **103** (2021), no. 2 023535, [[arXiv:2012.02518](#)].
- [49] H. V. Ragavendra, P. Saha, L. Sriramkumar, and J. Silk, *Primordial black holes and secondary gravitational waves from ultraslow roll and punctuated inflation*, *Phys. Rev. D* **103** (2021), no. 8 083510, [[arXiv:2008.12202](#)].
- [50] G. Franciolini and A. Urbano, *Primordial black hole dark matter from inflation: The reverse engineering approach*, *Phys. Rev. D* **106** (2022), no. 12 123519, [[arXiv:2207.10056](#)].
- [51] G. Domènech, G. Vargas, and T. Vargas, *An exact model for enhancing/suppressing primordial fluctuations*, *JCAP* **03** (2024) 002, [[arXiv:2309.05750](#)].
- [52] O. Özsoy and G. Tasinato, *On the slope of the curvature power spectrum in non-attractor inflation*, *JCAP* **04** (2020) 048, [[arXiv:1912.01061](#)].
- [53] S. Balaji, H. V. Ragavendra, S. K. Sethi, J. Silk, and L. Sriramkumar, *Observing Nulling of Primordial Correlations via the 21-cm Signal*, *Phys. Rev. Lett.* **129** (2022), no. 26 261301, [[arXiv:2206.06386](#)].
- [54] G. Franciolini, A. Iovino, Junior., M. Taoso, and A. Urbano, *One loop to rule them all: Perturbativity in the presence of ultra slow-roll dynamics*, [[arXiv:2305.03491](#)].
- [55] K.-W. Ng and Y.-P. Wu, *Constant-rate inflation: primordial black holes from conformal weight transitions*, *JHEP* **11** (2021) 076, [[arXiv:2102.05620](#)].
- [56] P. S. Cole, A. D. Gow, C. T. Byrnes, and S. P. Patil, *Steepest growth re-examined: repercussions for primordial black hole formation*, [[arXiv:2204.07573](#)].
- [57] N. Bhaumik and R. K. Jain, *Primordial black holes dark matter from inflection point models of inflation and the effects of reheating*, [[arXiv:1907.04125](#)]. [*JCAP*2001,037(2020)].
- [58] L. Iacconi, H. Assadullahi, M. Fasiello, and D. Wands, *Revisiting small-scale fluctuations in α -attractor models of inflation*, *JCAP* **06** (2022), no. 06 007, [[arXiv:2112.05092](#)].
- [59] M. Cicoli, F. G. Pedro, and N. Pedron, *Secondary GWs and PBHs in string inflation: formation and detectability*, *JCAP* **08** (2022), no. 08 030, [[arXiv:2203.00021](#)].
- [60] A. Karam, N. Koivunen, E. Tomberg, V. Vaskonen, and H. Veermäe, *Anatomy of single-field inflationary models for primordial black holes*, *JCAP* **03** (2023) 013, [[arXiv:2205.13540](#)].
- [61] W. Qin, S. R. Geller, S. Balaji, E. McDonough, and D. I. Kaiser, *Planck constraints and gravitational wave forecasts for primordial black hole dark matter seeded by multifield*

- inflation*, *Phys. Rev. D* **108** (2023), no. 4 043508, [[arXiv:2303.02168](#)].
- [62] M. Tagliazucchi, M. Braglia, F. Finelli, and M. Pieroni, *The quest of CMB spectral distortions to probe the scalar-induced gravitational wave background interpretation in PTA data*, [arXiv:2310.08527](#).
- [63] K. Kohri, D. H. Lyth, and A. Melchiorri, *Black hole formation and slow-roll inflation*, *JCAP* **0804** (2008) 038, [[arXiv:0711.5006](#)].
- [64] J. C. Mather et al., *Measurement of the Cosmic Microwave Background spectrum by the COBE FIRAS instrument*, *Astrophys. J.* **420** (1994) 439–444.
- [65] D. J. Fixsen, E. S. Cheng, J. M. Gales, J. C. Mather, R. A. Shafer, and E. L. Wright, *The Cosmic Microwave Background spectrum from the full COBE FIRAS data set*, *Astrophys. J.* **473** (1996) 576, [[astro-ph/9605054](#)].
- [66] C.-A. Faucher-Giguere, J. X. Prochaska, A. Lidz, L. Hernquist, and M. Zaldarriaga, *A direct precision measurement of the intergalactic Ly α opacity at $2 \leq z \leq 4.2$* , *The Astrophysical Journal* **681** (2008), no. 2 831.
- [67] V. F. Mukhanov, H. A. Feldman, and R. H. Brandenberger, *Theory of cosmological perturbations. Part 1. Classical perturbations. Part 2. Quantum theory of perturbations. Part 3. Extensions*, *Phys. Rept.* **215** (1992) 203–333.
- [68] J. Martin, *Inflationary cosmological perturbations of quantum-mechanical origin*, *Lect. Notes Phys.* **669** (2005) 199–244, [[hep-th/0406011](#)].
- [69] W. H. Kinney, *TASI Lectures on Inflation*, [arXiv:0902.1529](#).
- [70] D. Baumann, *Inflation*, in *Physics of the large and the small, TASI 09, proceedings of the Theoretical Advanced Study Institute in Elementary Particle Physics, Boulder, Colorado, USA, 1-26 June 2009*, pp. 523–686, 2011. [arXiv:0907.5424](#).
- [71] L. Sriramkumar, *An introduction to inflation and cosmological perturbation theory*, [arXiv:0904.4584](#).
- [72] P. Carrilho, K. A. Malik, and D. J. Mulryne, *Dissecting the growth of the power spectrum for primordial black holes*, *Phys. Rev. D* **100** (2019), no. 10 103529, [[arXiv:1907.05237](#)].
- [73] O. Özsoy, S. Parameswaran, G. Tasinato, and I. Zavala, *Mechanisms for Primordial Black Hole Production in String Theory*, *JCAP* **1807** (2018) 005, [[arXiv:1803.07626](#)].
- [74] O. Özsoy and G. Tasinato, *Consistency conditions and primordial black holes in single field inflation*, *Phys. Rev. D* **105** (2022), no. 2 023524, [[arXiv:2111.02432](#)].
- [75] J. Liu, Z.-K. Guo, and R.-G. Cai, *Analytical approximation of the scalar spectrum in the ultraslow-roll inflationary models*, *Phys. Rev. D* **101** (2020), no. 8 083535, [[arXiv:2003.02075](#)].
- [76] R. K. Jain, P. Chingangbam, J.-O. Gong, L. Sriramkumar, and T. Souradeep, *Punctuated inflation and the low CMB multipoles*, *JCAP* **01** (2009) 009, [[arXiv:0809.3915](#)].
- [77] R. K. Jain, P. Chingangbam, L. Sriramkumar, and T. Souradeep, *The tensor-to-scalar ratio in punctuated inflation*, *Phys. Rev. D* **82** (2010) 023509, [[arXiv:0904.2518](#)].
- [78] M. H. Qureshi, A. Iqbal, M. A. Malik, and T. Souradeep, *Low- ℓ power suppression in punctuated inflation*, *JCAP* **04** (2017) 013, [[arXiv:1610.05776](#)].
- [79] H. V. Ragavendra, D. Chowdhury, and L. Sriramkumar, *Suppression of scalar power on large scales and associated bispectra*, *Phys. Rev. D* **106** (2022), no. 4 043535, [[arXiv:2003.01099](#)].
- [80] **Planck** Collaboration, N. Aghanim et al., *Planck 2018 results. V. CMB power spectra and likelihoods*, *Astron. Astrophys.* **641** (2020) A5, [[arXiv:1907.12875](#)].
- [81] **BICEP**, **Keck** Collaboration, P. A. R. Ade et al., *Improved Constraints on Primordial*

Gravitational Waves using Planck, WMAP, and BICEP/Keck Observations through the 2018 Observing Season, *Phys. Rev. Lett.* **127** (2021), no. 15 151301, [[arXiv:2110.00483](#)].

- [82] **BOSS** Collaboration, S. Alam et al., *The clustering of galaxies in the completed SDSS-III Baryon Oscillation Spectroscopic Survey: cosmological analysis of the DR12 galaxy sample*, *Mon. Not. Roy. Astron. Soc.* **470** (2017), no. 3 2617–2652, [[arXiv:1607.03155](#)].
- [83] A. Drlica-Wagner, I. Sevilla-Noarbe, E. S. Rykoff, R. A. Gruendl, B. Yanny, D. L. Tucker, B. Hoyle, A. C. Rosell, G. M. Bernstein, K. Bechtol, M. R. Becker, A. Benoit-Lévy, E. Bertin, M. C. Kind, C. Davis, J. de Vicente, H. T. Diehl, D. Gruen, W. G. Hartley, B. Leistedt, T. S. Li, J. L. Marshall, E. Neilsen, M. M. Rau, E. Sheldon, J. Smith, M. A. Troxel, S. Wyatt, Y. Zhang, T. M. C. Abbott, F. B. Abdalla, S. Allam, M. Banerji, D. Brooks, E. Buckley-Geer, D. L. Burke, D. Capozzi, J. Carretero, C. E. Cunha, C. B. D’Andrea, L. N. da Costa, D. L. DePoy, S. Desai, J. P. Dietrich, P. Doel, A. E. Evrard, A. F. Neto, B. Flaugher, P. Fosalba, J. Frieman, J. García-Bellido, D. W. Gerdes, T. Giannantonio, J. Gschwend, G. Gutierrez, K. Honscheid, D. J. James, T. Jeltema, K. Kuehn, S. Kuhlmann, N. Kuropatkin, O. Lahav, M. Lima, H. Lin, M. A. G. Maia, P. Martini, R. G. McMahon, P. Melchior, F. Menanteau, R. Miquel, R. C. Nichol, R. L. C. Ogando, A. A. Plazas, A. K. Romer, A. Roodman, E. Sanchez, V. Scarpine, R. Schindler, M. Schubnell, M. Smith, R. C. Smith, M. Soares-Santos, F. Sobreira, E. Suchyta, G. Tarle, V. Vikram, A. R. Walker, R. H. Wechsler, J. Zuntz, and D. Collaboration), *Dark energy survey year 1 results: The photometric data set for cosmology*, *The Astrophysical Journal Supplement Series* **235** (apr, 2018) 33.
- [84] A. Lewis and S. Bridle, *Cosmological parameters from CMB and other data: A Monte Carlo approach*, *Phys. Rev. D* **66** (2002) 103511, [[astro-ph/0205436](#)].
- [85] A. Lewis, A. Challinor, and A. Lasenby, *Efficient computation of CMB anisotropies in closed FRW models*, *Astrophys. J.* **538** (2000) 473–476, [[astro-ph/9911177](#)].
- [86] A. Lewis, *GetDist: a Python package for analysing Monte Carlo samples*, [arXiv:1910.13970](#).
- [87] J. Chluba et al., *Spectral Distortions of the CMB as a Probe of Inflation, Recombination, Structure Formation and Particle Physics: Astro2020 Science White Paper*, *Bull. Am. Astron. Soc.* **51** (2019), no. 3 184, [[arXiv:1903.04218](#)].
- [88] **Planck** Collaboration, Y. Akrami et al., *Planck 2018 results. X. Constraints on inflation*, *Astron. Astrophys.* **641** (2020) A10, [[arXiv:1807.06211](#)].
- [89] S. Dodelson, *Modern Cosmology*. Academic Press, Elsevier Science, 2003.
- [90] R. Murgia, A. Merle, M. Viel, M. Totzauer, and A. Schneider, *“Non-cold” dark matter at small scales: a general approach*, *JCAP* **11** (2017) 046, [[arXiv:1704.07838](#)].
- [91] H. Bi and A. F. Davidsen, *Evolution of structure in the intergalactic medium and the nature of the $\text{Ly}\alpha$ forest*, *The Astrophysical Journal* **479** (1997), no. 2 523.
- [92] L. Hui and N. Y. Gnedin, *Equation of state of the photoionized intergalactic medium*, *Monthly Notices of the Royal Astronomical Society* **292** (1997), no. 1 27–42.
- [93] T. R. Choudhury, R. Srianand, and T. Padmanabhan, *Semianalytic approach to understanding the distribution of neutral hydrogen in the universe: comparison of simulations with observations*, *The Astrophysical Journal* **559** (2001), no. 1 29.
- [94] K. L. Pandey and S. K. Sethi, *Probing primordial magnetic fields using $\text{Ly}\alpha$ clouds*, *The Astrophysical Journal* **762** (2012), no. 1 15.
- [95] A. K. Sarkar, K. L. Pandey, and S. K. Sethi, *Using the redshift evolution of the $\text{Lyman-}\alpha$ effective opacity as a probe of dark matter models*, *Journal of Cosmology and Astroparticle Physics* **2021** (2021), no. 10 077.
- [96] S. Bird, H. V. Peiris, M. Viel, and L. Verde, *Minimally parametric power spectrum reconstruction from the Lyman α forest*, *MNRAS* **413** (May, 2011) 1717–1728,

- [arXiv:1010.1519].
- [97] T. Bringmann, P. Scott, and Y. Akrami, *Improved constraints on the primordial power spectrum at small scales from ultracompact minihalos*, *Phys. Rev. D* **85** (2012) 125027, [arXiv:1110.2484].
- [98] K. Kohri, T. Nakama, and T. Suyama, *Testing scenarios of primordial black holes being the seeds of supermassive black holes by ultracompact minihalos and CMB μ -distortions*, *Phys. Rev. D* **90** (2014), no. 8 083514, [arXiv:1405.5999].
- [99] T. Nakama, T. Suyama, K. Kohri, and N. Hiroshima, *Constraints on small-scale primordial power by annihilation signals from extragalactic dark matter minihalos*, *Phys. Rev. D* **97** (2018), no. 2 023539, [arXiv:1712.08820].
- [100] A. Kogut, D. J. Fixsen, D. T. Chuss, J. Dotson, E. Dwek, M. Halpern, G. F. Hinshaw, S. M. Meyer, S. H. Moseley, M. D. Seiffert, D. N. Spergel, and E. J. Wollack, *The Primordial Inflation Explorer (PIXIE): a nulling polarimeter for cosmic microwave background observations*, *JCAP* **2011** (July, 2011) 025, [arXiv:1105.2044].
- [101] R.-g. Cai, S. Pi, and M. Sasaki, *Gravitational Waves Induced by non-Gaussian Scalar Perturbations*, *Phys. Rev. Lett.* **122** (2019), no. 20 201101, [arXiv:1810.11000].
- [102] C. Unal, *Imprints of Primordial Non-Gaussianity on Gravitational Wave Spectrum*, *Phys. Rev. D* **99** (2019), no. 4 041301, [arXiv:1811.09151].
- [103] V. Atal and G. Domènech, *Probing non-Gaussianities with the high frequency tail of induced gravitational waves*, *JCAP* **06** (2021) 001, [arXiv:2103.01056]. [Erratum: *JCAP* **10**, E01 (2023)].
- [104] P. Adshead, K. D. Lozanov, and Z. J. Weiner, *Non-Gaussianity and the induced gravitational wave background*, *JCAP* **10** (2021) 080, [arXiv:2105.01659].
- [105] F. Zhang, J. Lin, and Y. Lu, *Double-peaked inflation model: Scalar induced gravitational waves and primordial-black-hole suppression from primordial non-Gaussianity*, *Phys. Rev. D* **104** (2021), no. 6 063515, [arXiv:2106.10792]. [Erratum: *Phys.Rev.D* **104**, 129902 (2021)].
- [106] H. V. Ragavendra, *Accounting for scalar non-Gaussianity in secondary gravitational waves*, *Phys. Rev. D* **105** (2022), no. 6 063533, [arXiv:2108.04193].
- [107] S. Garcia-Saenz, L. Pinol, S. Renaux-Petel, and D. Werth, *No-go theorem for scalar-trispectrum-induced gravitational waves*, *JCAP* **03** (2023) 057, [arXiv:2207.14267].
- [108] C. Chen, A. Ota, H.-Y. Zhu, and Y. Zhu, *Missing one-loop contributions in secondary gravitational waves*, [arXiv:2210.17176].
- [109] J.-P. Li, S. Wang, Z.-C. Zhao, and K. Kohri, *Primordial non-Gaussianity f_{NL} and anisotropies in scalar-induced gravitational waves*, *JCAP* **10** (2023) 056, [arXiv:2305.19950].
- [110] G. Franciolini, A. Iovino, Junior., V. Vaskonen, and H. Veermae, *Recent Gravitational Wave Observation by Pulsar Timing Arrays and Primordial Black Holes: The Importance of Non-Gaussianities*, *Phys. Rev. Lett.* **131** (2023), no. 20 201401, [arXiv:2306.17149].
- [111] L. Liu, Z.-C. Chen, and Q.-G. Huang, *Implications for the non-Gaussianity of curvature perturbation from pulsar timing arrays*, *Phys. Rev. D* **109** (2024), no. 6 L061301, [arXiv:2307.01102].
- [112] C. Yuan, D.-S. Meng, and Q.-G. Huang, *Full analysis of the scalar-induced gravitational waves for the curvature perturbation with local-type non-Gaussianities*, *JCAP* **12** (2023) 036, [arXiv:2308.07155].
- [113] J.-P. Li, S. Wang, Z.-C. Zhao, and K. Kohri, *Complete Analysis of Scalar-Induced Gravitational Waves and Primordial Non-Gaussianities f_{NL} and g_{NL}* , [arXiv:2309.07792].
- [114] S. Choudhury, K. Dey, A. Karde, S. Panda, and M. Sami, *Primordial non-Gaussianity as a*

saviour for PBH overproduction in SIGWs generated by Pulsar Timing Arrays for Galileon inflation, [arXiv:2310.11034](#).

- [115] Z. Chang, Y.-T. Kuang, D. Wu, J.-Z. Zhou, and Q.-H. Zhu, *New constraints on primordial non-Gaussianity from missing two-loop contributions of scalar induced gravitational waves*, *Phys. Rev. D* **109** (2024), no. 4 L041303, [[arXiv:2311.05102](#)].
- [116] R. Inui, S. Jaraba, S. Kuroyanagi, and S. Yokoyama, *Constraints on Non-Gaussian primordial curvature perturbation from the LIGO-Virgo-KAGRA third observing run*, [arXiv:2311.05423](#).
- [117] Z. Chang, Y.-T. Kuang, D. Wu, and J.-Z. Zhou, *Probing scalar induced gravitational waves with PTA and LISA: The Importance of third order correction*, [arXiv:2312.14409](#).
- [118] T. Papanikolaou, X.-C. He, X.-H. Ma, Y.-F. Cai, E. N. Saridakis, and M. Sasaki, *New probe of non-Gaussianities with primordial black hole induced gravitational waves*, [arXiv:2403.00660](#).
- [119] C. T. Donnan, D. J. McLeod, J. S. Dunlop, R. J. McLure, A. C. Carnall, R. Begley, F. Cullen, M. L. Hamadouche, R. A. A. Bowler, D. Magee, H. J. McCracken, B. Milvang-Jensen, A. Moneti, and T. Targett, *The evolution of the galaxy UV luminosity function at redshifts $z \simeq 8 - 15$ from deep JWST and ground-based near-infrared imaging*, *Monthly Notices of the Royal Astronomical Society* **518** (Feb., 2023) 6011–6040, [[arXiv:2207.12356](#)].
- [120] I. Labbé, P. van Dokkum, E. Nelson, R. Bezanson, K. A. Suess, J. Leja, G. Brammer, K. Whitaker, E. Mathews, M. Stefanon, and B. Wang, *A population of red candidate massive galaxies 600 Myr after the Big Bang*, *Nature* **616** (Apr., 2023) 266–269, [[arXiv:2207.12446](#)].
- [121] W.-C. Syu, D.-S. Lee, and K.-W. Ng, *Quantum loop effects to the power spectrum of primordial perturbations during ultra slow-roll inflation*, *Phys. Rev. D* **101** (2020), no. 2 025013, [[arXiv:1907.13089](#)].
- [122] J. Kristiano and J. Yokoyama, *Ruling Out Primordial Black Hole Formation From Single-Field Inflation*, [arXiv:2211.03395](#).
- [123] K. Inomata, M. Braglia, X. Chen, and S. Renaux-Petel, *Questions on calculation of primordial power spectrum with large spikes: the resonance model case*, *JCAP* **04** (2023) 011, [[arXiv:2211.02586](#)]. [Erratum: *JCAP* 09, E01 (2023)].
- [124] S. Choudhury, M. R. Gangopadhyay, and M. Sami, *No-go for the formation of heavy mass Primordial Black Holes in Single Field Inflation*, [arXiv:2301.10000](#).
- [125] H. Firouzjahi, *Revisiting Loop Corrections in Single Field USR Inflation*, [arXiv:2311.04080](#).
- [126] S.-L. Cheng, D.-S. Lee, and K.-W. Ng, *Primordial perturbations from ultra-slow-roll single-field inflation with quantum loop effects*, [arXiv:2305.16810](#).
- [127] S. Choudhury, S. Panda, and M. Sami, *Quantum loop effects on the power spectrum and constraints on primordial black holes*, [arXiv:2303.06066](#).
- [128] S. Maity, H. V. Ragavendra, S. K. Sethi, and L. Sriramkumar, *Loop contributions to the scalar power spectrum due to quartic order action in ultra slow roll inflation*, [arXiv:2307.13636](#).
- [129] A. Riotto, *The Primordial Black Hole Formation from Single-Field Inflation is Not Ruled Out*, [arXiv:2301.00599](#).
- [130] H. Firouzjahi and A. Riotto, *Primordial Black Holes and Loops in Single-Field Inflation*, [arXiv:2304.07801](#).
- [131] J. Fumagalli, *Absence of one-loop effects on large scales from small scales in non-slow-roll dynamics*, [arXiv:2305.19263](#).
- [132] S.-L. Cheng, D.-S. Lee, and K.-W. Ng, *Power spectrum of primordial perturbations during ultra-slow-roll inflation with back reaction effects*, *Phys. Lett. B* **827** (2022) 136956, [[arXiv:2106.09275](#)].